International Journal of Rock Mechanics & Mining Sciences 160 (2022) 105238

Contents lists available at ScienceDirect

International Journal of Rock Mechanics and Mining Sciences

journal homepage: www.elsevier.com/locate/ijrmms

Technical Note

Space-time effect of blasting stress wave and blasting gas on rock fracture based on a cavity charge structure

Chenxi Ding [a,b,d], Renshu Yang [a,b,*], Cheng Chen [a,b], Xinguang Zhu [c], Chun Feng [c], Quanmin Xie [d]

[a] School of Civil and Resource Engineering, University of Science and Technology Beijing, Beijing, 100083, China
[b] Key Laboratory of Ministry of Education for High-Efficient Mining and Safety of Metal Mines, University of Science and Technology Beijing, Beijing, 100083, China
[c] Key Laboratory for Mechanics in Fluid Solid Coupling Systems, Institute of Mechanics, Chinese Academy of Sciences, Beijing, 100190, China
[d] Hubei Key Laboratory of Blasting Engineering of Jianghan University, Wuhan, 430056, China

ARTICLE INFO

Keywords:
Blasting stress wave
Blasting gas
Cavity charge structure
Strain evolution
Crack propagation

ABSTRACT

There are still varying opinions on the relative spatio-temporal contributions of blasting stress wave and blasting gas in the theoretical study of rock blasting due to the transient nature of the blasting process and the complexity of the blasting effect. Based on this, the study proposes a cavity charge structure entailing quantitative and differentiated research on the effects of blasting stress wave and blasting gas over time and space. The time and space action characteristics of blasting gas are regulated by changing the charge structure of the borehole and placing a cavity between the charge and borehole wall, and the "double-peak" evolution law of blasting strain is obtained. The first peak is generated by blasting stress wave, and the second peak is generated by blasting gas, with a delay between the first and second peaks. Further analysis shows that the cavity has different effects on blasting stress wave and blasting gas. Finally, the space-time effect of blasting stress wave and blasting gas can be fully utilized to achieve controllable rock fragmentation by adjusting the charge position and the cavity volume in the cavity charge structure.

1. Introduction

Blasting stress wave and blasting gas are the main driving forces involved in rock fragmentation during the blasting process. Elucidating the effect of blasting stress wave and blasting gas is essential for revealing the basic theory of rock blasting. The rock fragmentation theory regarding blasting stress wave and blasting gas have evolved over the past years. The initial theories had divided opinions on which component of blasting phenomenon was the main contributor of rock fragmentation. Some proposed that the blast stress waves were the driving force while other considered it to be the blasting gases.[1,2] Later, after decades of academic debate, researchers came to a conclusion that both had significant roles in the rock fragmentation, thus establishing a comprehensive action theory of blasting stress wave and blasting gas,[3,4] and is recognized by the majority. This theory states that the action of blasting stress wave is the main reason for the formation of initial cracks in the rock,[5] and the quasi-static effect of blasting gas further expands some of the cracks formed by the stress wave.[6] Researchers continue to this day to enrich and develop the connotation of the comprehensive action theory in order to further improve the basic theory of rock blasting.[7–10]

Both the wave characteristics of the blasting stress wave[11] and the pressure change of blasting gas[12] significantly affect the generation and propagation of blast-induced cracks, which in turn determine the rock fragmentation effect. Many researchers are attempting to separate blasting stress wave and blasting gas in order to perform independent studies on the mechanisms of rock fragmentation. However, in the physical process of blasting, the blasting stress wave and blasting gas are generated simultaneously, which makes conducting individual research extremely challenging. Therefore, in terms of model experiments, some equivalent treatment methods are adopted to study the dynamic effects of blasting stress wave by shielding blasting gas,[13,14] or to study the energy distribution of blasting gas by ignoring the effect of blasting stress wave.[15] It is undeniable that such research methods help in gaining further understanding of the effects of blasting stress wave and blasting gas, but it is difficult to support them in the context of scientific experimental design. In recent years, numerical simulation has taken over as the primary technique for analyzing the effects of blasting stress

* Corresponding author. School of Civil and Resource Engineering, University of Science and Technology Beijing, Beijing, 100083, China.
E-mail address: yrs@ustb.edu.cn (R. Yang).

https://doi.org/10.1016/j.ijrmms.2022.105238
Received 4 July 2022; Received in revised form 28 September 2022; Accepted 11 October 2022
Available online 17 October 2022

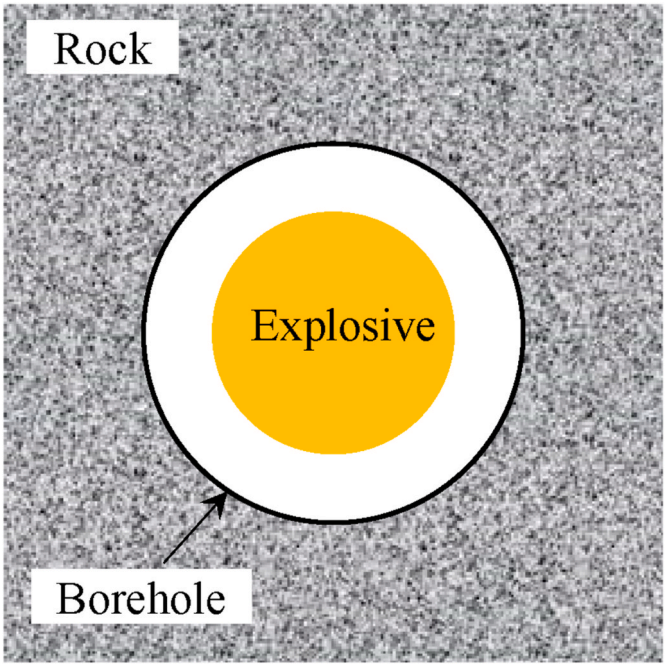

Fig. 1. Decoupling charge structure.

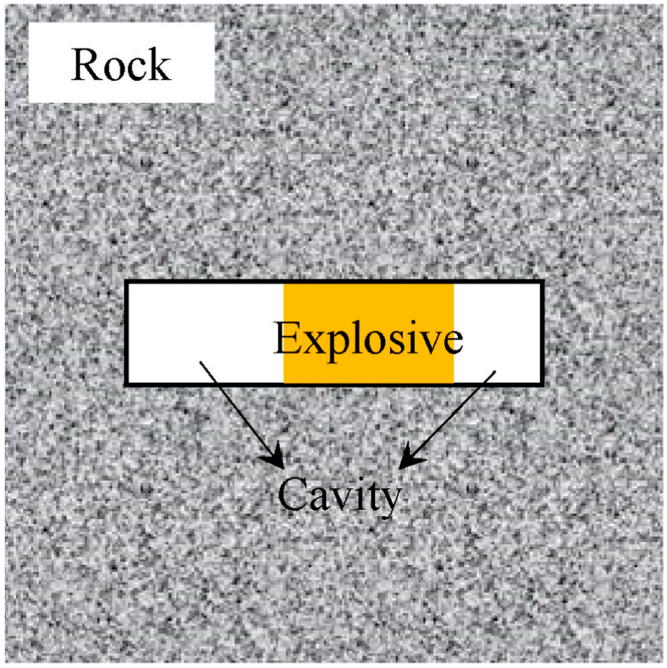

Fig. 2. Cavity charge structure.

waves and blasting gas due to the complexity of experimental research. The loading characteristics of blasting stress wave are simulated by applying different load curves to the borehole wall,[16–18] and the effect of blasting gas is analyzed by controlling the corresponding relationship between gas volume and pressure in the blast-induced crack.[19–21] However, the research results of numerical simulation also have certain limitations. The existing numerical simulation techniques adopt a lot of equivalence laws and simplification, making it impossible to realistically simulate the physical process of rock fragmentation induced by blasting stress wave and blasting gas. Further, it lacks reliable experimental verification.

There are still numerous shortcomings in the existing research on the rock fragmentation mechanism of blasting stress wave and blasting gas. In terms of model experiment research, considering the physical process of blasting, the idea of separating blasting stress wave and blasting gas and conducting research independently will remain scientifically questionable. Therefore, this paper proposes a cavity charge structure that distinguishes the effects of blasting stress wave and blasting gas over the time and space scales, allowing for the identification and quantitative analysis of the two.

2. Cavity charge structure and experimental design

2.1. Mechanics of the decoupling charge structure

The decoupling charge structure depicted in Fig. 1 is a technical method for controlling the impacts of blasting stress wave and blasting gas used in engineering practices. For decoupling charge blasting, the rock blasting theory holds that the detonation wave and high-pressure blasting gas generated after detonation first compresses the filling medium between borehole wall and explosive, and then acts on the borehole wall after being buffered by the filling medium and transfers the blasting energy to the rock, which can avoid excessive rock fragmentation.[22] According to a previous study,[23] the blasting stress evolution characteristics in decoupling charge blasting are not significantly different from those generated in coupling charge blasting. The stress/strain time history curves are all typical “single peak” curves, but the stress peak and decay characteristics are different. Although decoupling charge blasting is widely considered to effectively adjust the effects of blasting stress wave and blasting gas, it is still difficult to understand the rock fragmentation characteristics of blasting stress wave and blasting gas through decoupling charge structure. This is mainly due to the fact that the explosive is located in the center of the borehole in the decoupling charge structure. Thus, the blasting stress wave and blasting gas act on the filling medium at the same time, and the effects of the two are mixed together over time and space. It is impossible to distinguish their respective contributions to the rock stress characteristics and fracture degree.

2.2. Proposition of the cavity charge structure

Based on the concept of the decoupling charge structure, the experimental design focuses on how to separate the effects of blasting stress wave and blasting gas in the blasted medium over the time and space scales. Inspired by the decoupling charge structure, a cavity charge structure is proposed herein, as shown in Fig. 2, which involves changing the borehole shape and the explosive position in borehole. For the two-dimensional plane model experiment, the shape of borehole is set as a rectangle, and a rectangular charge with the same width as borehole is placed in the borehole. The upper and lower sides of the charge are in direct contact with the borehole wall, and there are cavities between the left and right sides of the charge and borehole wall. After the charge is detonated, the detonation wave acts immediately on the upper and lower sides of the borehole wall and then propagates in the blasted medium in the form of blasting stress waves. The blasting gas diffuses in the cavity and then acts on the left and right sides of the borehole wall. Under the condition of such a charge structure, the effects of detonation wave and blasting gas on the blasted medium is different in time and space. The following is a one-dimensional flow analysis of the diffusion of blasting gas over the time and space scales.

An explosive with a length of l is placed in the rigid wall tube, the detonation velocity of the explosive is D, and the left end of the explosive is vacuum. When the explosive is detonated from the left end, the detonation wave propagates to the right at the speed D, and the blasting gas (detonation product) behind the detonation wave front rapidly expands and scatters to the left, forming a cluster of rarefaction waves that closely follows the C-J plane and propagates to the right. According to the one-dimensional isentropic flow theory of gas, the one-dimensional

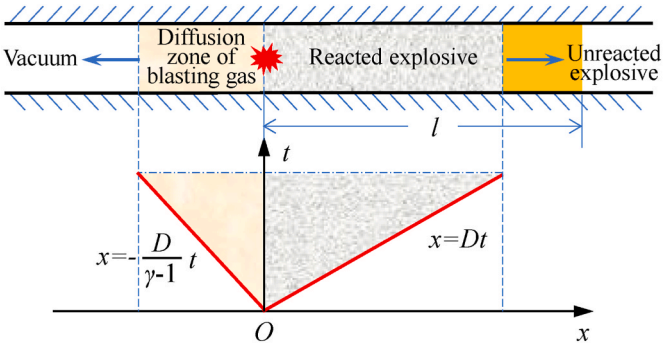

Fig. 3. Schematic diagram of one-dimensional flow of blasting gas.

isentropic motion law of blasting gas satisfies the following equation[24]:

$$\begin{cases} \dfrac{\partial}{\partial t}\left(v+\dfrac{2c}{\gamma-1}\right)+(v+c)\dfrac{\partial}{\partial x}\left(v+\dfrac{2c}{\gamma-1}\right)=0 \\ \dfrac{\partial}{\partial t}\left(v-\dfrac{2c}{\gamma-1}\right)+(v-c)\dfrac{\partial}{\partial x}\left(v-\dfrac{2c}{\gamma-1}\right)=0 \end{cases} \tag{1}$$

where t is the time; x is the displacement of blasting gas; c is the velocity of sound in blasting gas; v is the flow velocity of blasting gas; γ is the specific heat ratio of blasting gas.

The rarefaction waves propagating to the right following the detonation wave are a cluster of right-propagating simple waves. This cluster of rarefaction waves can be described using the special solution of Eq. (1) as:

$$\begin{cases} x=(v+c)t+F_1(v) \\ v-\dfrac{2c}{\gamma-1}=\text{constant} \end{cases} \tag{2}$$

where F_1 is an arbitrary function, which is determined by the initial conditions. The detonation time is $t=0$, and the detonation position is $x=0$, thus $F_1=0$.

The parameter of the blasting gas immediately after the detonation wave front is the C-J parameter, where the propagation velocity of blasting gas is $\frac{1}{\gamma+1}D$, and the velocity of sound is $\frac{\gamma}{\gamma+1}D$. Thus, the solution of Eq. (2) is obtained as:

$$\begin{cases} v=\dfrac{2}{\gamma+1}\dfrac{x}{t}-\dfrac{1}{\gamma+1}D \\ c=\dfrac{\gamma-1}{\gamma+1}\dfrac{x}{t}+\dfrac{1}{\gamma+1}D \end{cases} \tag{3}$$

Since the left side of the detonation position is a vacuum, $c=0$ at the wave head of the blasting gas propagating to the left. According to Eq. (3), the equation of motion of the blasting gas propagating to the left is:

$$x=-\frac{1}{\gamma-1}Dt \tag{4}$$

The schematic picture of one-dimensional blasting gas flow depicted in Fig. 3 is generated by combining the preceding analytical findings. After the explosive is detonated, the blasting gas rapidly expands to the left, and its diffusion velocity becomes $\frac{1}{\gamma-1}D$. For high-energy explosives, the specific heat ratio of blasting gas is $\gamma\approx 3$. Therefore, theoretical analysis shows that the blasting gas diffusion velocity is about half of the detonation velocity. In the model experimental design performed in the present study, there is air instead of vacuum in the cavities on the left and right sides of the explosive. The blasting gas compresses the air in the cavity during the diffusion process, resulting in a further decrease in the diffusion velocity. Thus, the cavities on the left and right sides of the explosive delay the effect of blasting gas on the borehole wall, and distinguish the impact of detonation wave and blasting gas on the borehole wall from the time scale.

2.3. Experimental design and parameters

Based on the cavity charge structure, the experimental design shown in Fig. 4 is developed. A rectangular borehole with a length of 20 mm and a width of 4 mm is prefabricated in the middle of the test piece. The borehole is divided into five equal parts along the length direction. The explosive is placed in the shape of a 4 mm × 4 mm square charge. Further, there are three relative positions of the charge in the borehole. There are obvious differences in the constraints between the charge and the borehole under these three position conditions. Specimen S1: The upper, lower, and left sides of the charge are in direct contact with the borehole wall, and the right side of the charge opens to the cavity. Specimen S2: The upper and lower sides of the charge are in direct contact with the borehole wall, while the left and right sides of the charge face the cavities. Specimen S3: Both the upper and lower sides of the charge are in direct contact with the borehole wall, and the left and right sides of the charge are facing the cavities. In contrast to Specimen S2, the lengths of the cavities on both sides of Specimen S3 are the same.

The total volume of the cavities on the left and right sides of the charge is the same in all three specimen groups mentioned above and is recorded as 4V. In the case of specimen S1, the volume of the cavity on the left side of the charge is 0, and the volume of the cavity on the right side is 4V. For specimen S2, the volume of the cavity on the left side of the charge is V, whereas the volume of the cavity on the right side is 3V. For specimen S3, the volume of the cavity on the left and right sides of

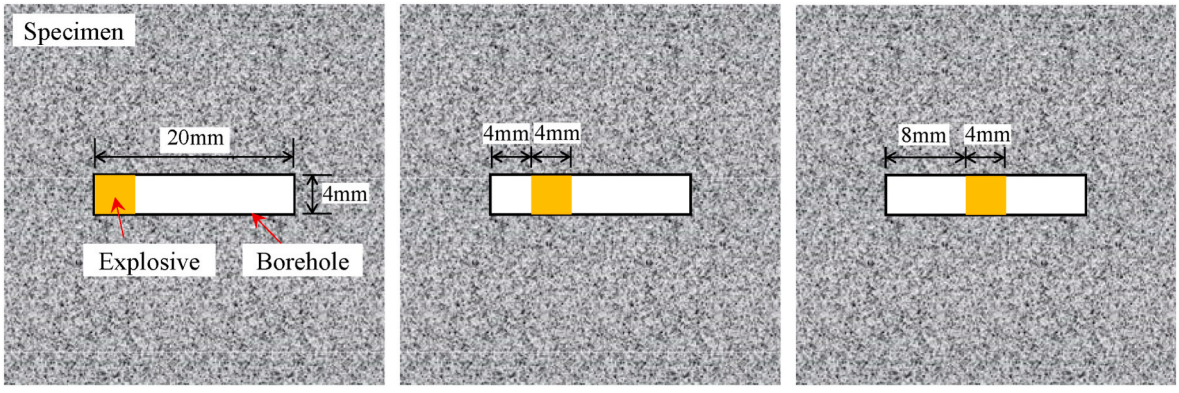

Fig. 4. Schematic diagram of specimens.

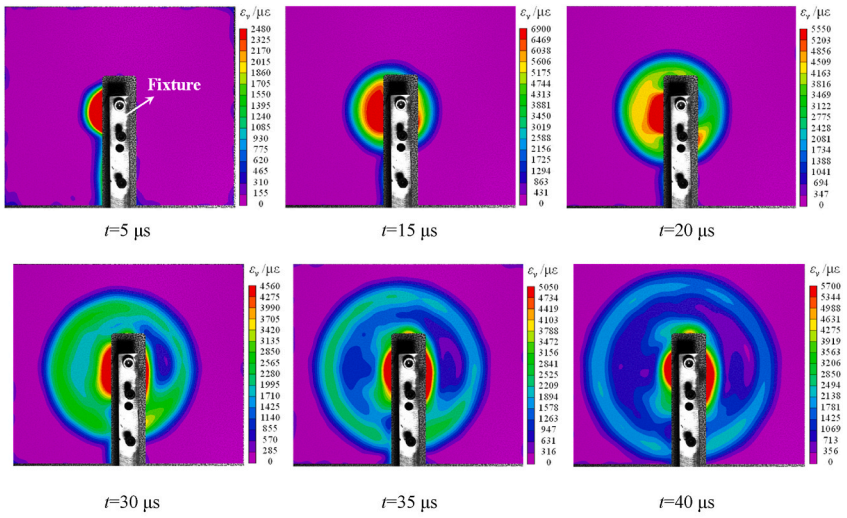

(a) Specimen S1

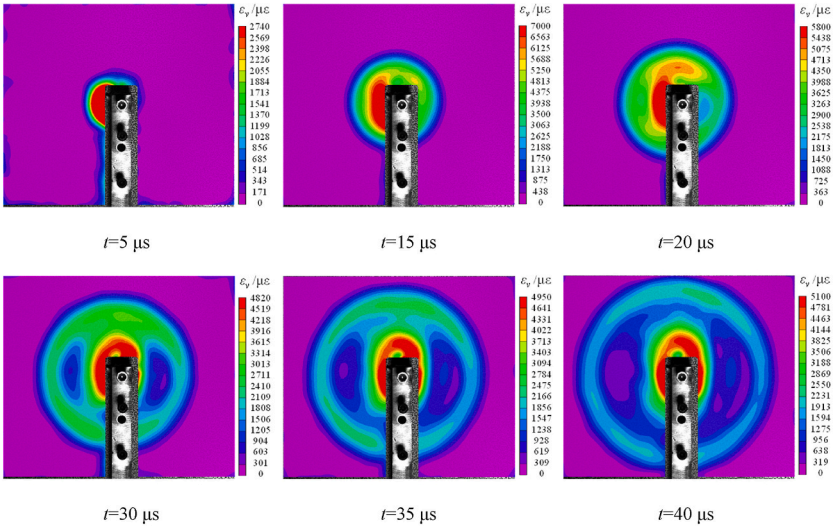

(b) Specimen S2

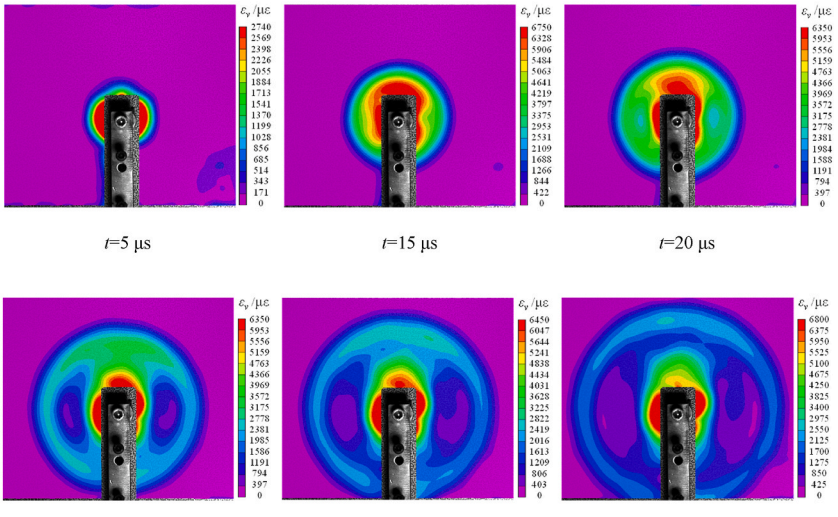

(c) Specimen S3

Fig. 5. Cloud map of Mises strain evolution in each specimen group.

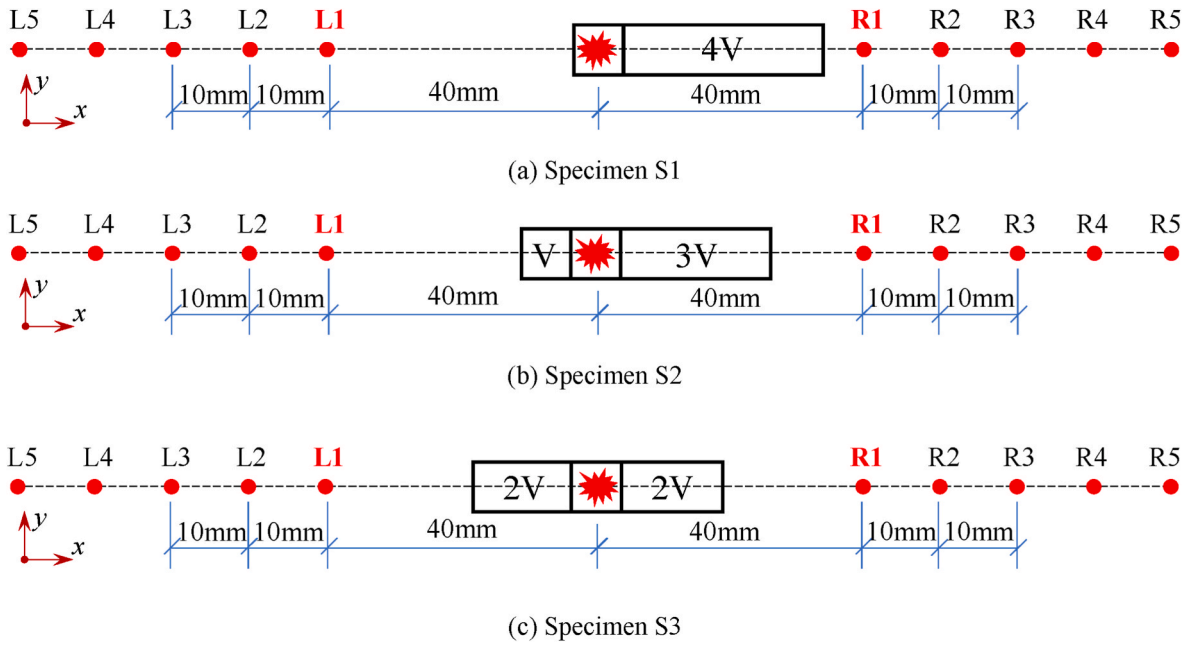

Fig. 6. Schematic diagram of gauging point position in the borehole.

the charge is both 2V. The explosive used in the experiment is lead azide, and the charge of a single borehole is 120 mg. The specific volume, detonation temperature, and detonation velocity of lead azide are respectively 308 L/kg, 3050 °C and 4478 m/s. Additionally, two specimen materials, polycarbonate (PC) and polymethyl methacrylate (PMMA) are employed to analyze the evolution of blasting strain and the propagation of blast-induced cracks, respectively. The elastic modulus and Poisson's ratio of PC are respectively 4.5 GPa and 0.32. The elastic modulus and Poisson's ratio of PMMA are respectively 6.1 GPa and 0.31. PC is used as the specimen material for studying the blasting strain evolution. The blasting process is photographed and recorded by a high-speed camera, and the evolution process of the blasting strain field is calculated by combining the digital image correlation method. When studying the propagation of blast-induced cracks, PMMA is used as the specimen material to observe and analyze the distribution state of blast-induced cracks.

3. Analysis of blasting strain

3.1. Blasting strain evolution

In the experiment, the borehole is blocked with a special fixture to prevent the premature leakage of blasting gas. The blasting process is photographed and recorded by a high-speed camera. The shooting speed of the high-speed camera is set to 1000000 fps, that is, the time interval between two successive photos is 1 μs. The Mises strain evolution cloud map of specimen S1 is shown in Fig. 5(a), where the explosive detonation time is assumed to be $t = 0$ s. In the figure, the warm-toned area represents the high-strain area, and the cool-toned area represents the low-strain area. After the explosive is detonated, the circular strain field spreads to the periphery with the charge as the center. It can be seen from the figure that in the early stages of blasting strain evolution, the strain value in the area on the left side of borehole is significantly higher than that on the right side of borehole. This is mainly due to the charge's proximity to the left borehole wall. When the explosive is detonated, the detonation wave directly acts on the left borehole wall, thus the left area of borehole is subjected to greater stress in the early stage. In the later stage, the stress states on the left and right sides of borehole tend to reach equilibrium. It can be seen that the shape of the charge has a significant effect on the evolution of blasting stress. Fig. 5(b) shows the Mises strain evolution cloud map of specimen S2. Although the charge is not in touch with the left or right borehole walls, there is a comparatively small gap between the charge and the left borehole wall, which causes a relatively high initial strain value on the left side of the borehole. Fig. 5(c) shows the Mises strain evolution cloud map of specimen S3. It can be seen that the strain distribution on the left and right sides of the borehole is relatively uniform. This is because the cavity size on the left and right sides of the charge is the same so the stress state on both sides of the borehole is basically symmetrical.

3.2. Blasting strain peak

In order to further study the evolution process of blasting strain, the strain curves measured at relevant gauging points are extracted for analysis. As shown in Fig. 6, five gauging points are selected on the left side of borehole, namely L1, L2, L3, L4, and L5. The distance between two adjacent gauging points is 10 mm, and the distance from L1 to the charge center is 40 mm. Similarly, five gauging points are selected on the right side of borehole as well, namely R1, R2, R3, R4, and R5. The distance between two adjacent gauging points is 10 mm, and the distance from R1 to the charge center is also 40 mm.

The gauging points L1 and R1 are located on the left and right sides of the borehole, respectively, and the distances between them and the charge center are equal. For specimen S1, the left side of the charge is in direct contact with the borehole wall, and the cavity volume on the left side of charge is 0. For the convenience of subsequent analysis, the gauging points on the left side of borehole are labeled as 0-L1, 0-L2, 0-L3, 0-L4, and 0-L5 in sequence. The cavity volume on the right side of charge for specimen S1 is 4V, thus the gauging points on the right side of borehole are recorded as 4V-R1, 4V-R2, 4V-R3, 4V-R4, and 4V-R5, respectively. Similarly, for specimen S2, the gauging points on the left side of borehole are recorded as V-L1, V-L2, V-L3, V-L4, and V-L5 in sequence, and the gauging points on the right side of borehole are recorded as 3V-R1, 3V-R2, 3V-R3, 3V-R4, and 3V-R5. For specimen S3, the volume of the cavity on the left and right sides of the charge is 2V. Therefore, considering the symmetry of this specimen only the gauging point on the right side of borehole is taken for analysis. The gauging points on the right side of borehole are recorded as 2V-R1, 2V-R2, 2V-R3, 2V-R4, and 2V-R5.

The strain evolution analysis will be carried out on the gauging

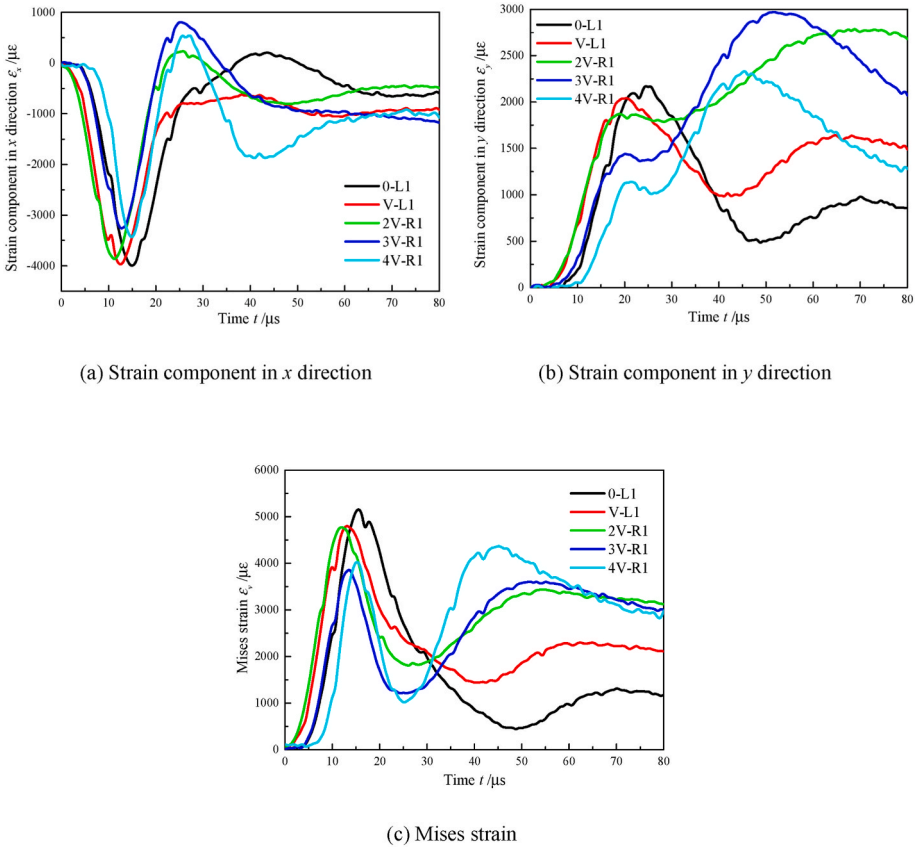

(a) Strain component in x direction

(b) Strain component in y direction

(c) Mises strain

Fig. 7. Strain curves of relevant gauging points.

points L1 and R1 on the left and right sides of borehole in the subsequent analysis. Fig. 7 shows the strain curves measured at the gauging points L1 and R1 for all the three groups of specimens considered. The negative strain indicates that the gauging point is under compression, and the positive strain indicates that the gauging point is under tension. The strain component in x direction is dominated by compression, whereas the strain component in y direction is dominated by tension. The compressive strain in x direction is significantly larger than the tensile strain in y direction. Mises strain is an equivalent strain, which can comprehensively reflect the stress state of the material at the gauging point. The strain curves of the relevant gauging points exhibit a "double-peak" evolution characteristic, which is significantly different from the strain evolution law observed in coupling and decoupling charge blastings.

It can be seen from Fig. 7 that the strain curves at different gauging points essentially reach the first strain peak at the same time, but there are significant differences in the corresponding time to reach the second strain peak. As mentioned earlier, in all three groups of specimens, the charge is in direct contact with the upper and lower sides of the borehole. When the explosive is detonated, the shock wave directly impinges on the upper and lower sides of borehole walls and then attenuates into a blasting stress wave in the specimen. It continues to propagate as blasting stress wave and is recorded at the various gauging points. The propagation velocity of blasting stress wave in the specimen is a determined value, and the distances between the gauging points, L1 and R1, of the relevant specimen to the charge center are equal. Therefore, the time for the blasting stress wave to propagate and act on the relevant gauging points is nearly identical. In conjunction with the calculation and verification of distance and wave velocity, it is also established that the first strain peak is the result of the blasting stress wave. In addition, the relative position of the charge in borehole affects the reflection and transmission of the blasting stress wave at the upper and lower sides of the borehole wall. This explains the difference in the propagation intensity of blasting stress wave, and consequently the difference in the value of the first strain peak of the relevant gauging points.

The high-pressure blasting gas generated by the detonation of the explosive diffuses to the cavities on the left and right sides of the charge. The blasting gas compresses the air in the cavity during the diffusion process, following which the blasting gas and the compressed air impact the left and right sides of borehole wall. The stress wave generated by this impact on borehole wall propagates in the specimen and acts on the relevant gauging points again, which promotes the generation of the second strain peak. On the one hand, due to the difference in the cavity volume, the diffusion velocity of blasting gas and the compression degree of air are different. Whereas, the distances from the relevant gauging points to borehole wall are different as well, resulting in a variation in blasting stress attenuation. The two aforementioned factors result in considerable changes in the magnitude of the second strain peak value of the relevant gauging points under the action of blasting gas.

The time it takes for the blasting gas to disperse and compress the air in the cavity is quite long when compared to the action time of the detonation wave. This distinguishes the impact of blasting gas on borehole walls and the effect of detonation wave over the time and space scales. Thus, the distinction study of the effect of blasting stress wave and blasting gas is achieved at the experimental level. Furthermore, the strain curve shows that the stress duration of the relevant gauging point under the action of blasting gas is longer, which is favorable for the propagation of blast-induced cracks.

Tensile stress has the greatest influence on rock fragmentation and crack propagation during blasting. The x direction is dominated by compression at the gauging points on the left and right sides of borehole, whereas the y direction is dominated by tension. Therefore, the strain component in y direction of the gauging point L1 or R1 of the three

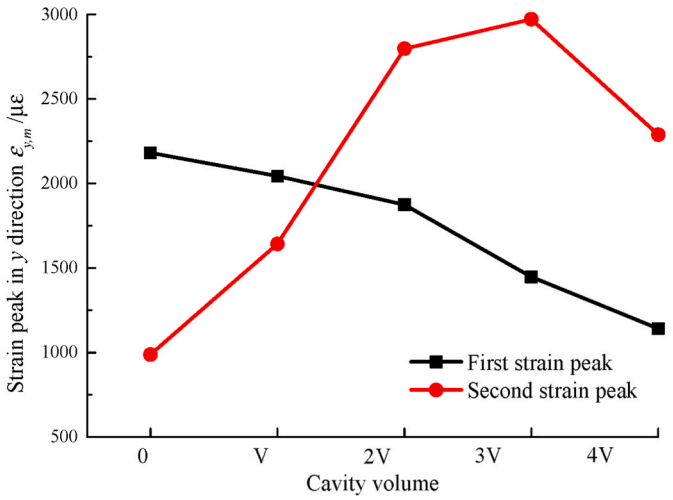

Fig. 8. Changing curve of strain peak in y direction with cavity volume.

specimens is compared and analyzed herein. Fig. 8 shows the changing curve of strain peak in y direction with cavity volume. The first strain peak decreases with the increase of cavity volume, while the second strain peak increases first and then decreases with the increase of cavity volume. The maximum value of the first strain peak is obtained when the cavity volume is 0, which is 2181 με. The maximum value of the second strain peak is obtained when the cavity volume is 3V, which is 2973 με. When the cavity volume is small (0 or V), the first strain peak is significantly higher than the second strain peak, and the effect of blasting stress wave is dominant. When the cavity volume is large (≥2V), the first strain peak is clearly lower than the second strain peak, and the effect of blasting gas dominates. In general, as far as the stress state at the gauging point is concerned, with the increase of cavity volume, the effect of blasting stress wave gradually weakens, while the effect of blasting gas gradually increases. Furthermore, the excessively large cavity volume reduces the effect of blasting stress wave, while inhibiting the effect of blasting gas. It is evident that a reasonable cavity volume can adjust the space-time effect of blasting stress wave and blasting gas, and control the stress state of the blasted medium, so as to achieve a better blasting effect.

In order to further explore the attenuation law of the strain peak under the action of blasting stress wave and blasting gas, the strain peak in y direction of the gauging points on the left and right sides of the cavity is measured and fitted to obtain the attenuation curve shown in Fig. 9. The attenuation of strain peak at gauging points is nonlinear, and the attenuation law satisfies the following equation:

$$\varepsilon_{y,m} = a/s^{-n} \tag{5}$$

where $\varepsilon_{y,m}$ is the strain peak in y direction; a is the proportionality coefficient; s is the distance from the gauging point to the charge center; n is the attenuation index.

The attenuation index n characterizes the strain attenuation rate of the gauging point. The attenuation index under different cavity volume settings is calculated using the strain peak fitting curve in Fig. 9, as reported in Table 1. According to the data in the table, the attenuation index of the second strain peak is much lower than that of the first strain peak, suggesting that the second strain peak, which is dominated by blasting gas, undergoes a more rapid attenuation.

4. Analysis of blast-induced crack

In order to further explore the distribution characteristics of blast-induced cracks in the cavity charge structure, a blasting model experiment is carried out with PMMA as the experimental material. Borehole parameters, charge parameters, and charge position are consistent with the previous experiments, and corresponding specimens are recorded as Specimen T1, Specimen T2, and Specimen T3. Fig. 10 is a schematic diagram of the distribution of blast-induced cracks around borehole after blasting. The four corners of the borehole are predicted to have a stress concentration effect during blasting and form the blast-induced crack, which is denoted as Crack A. Moreover, in order to study the crack propagation behavior on the left and right sides of borehole, prefabricated cracks are made on the left and right sides of borehole, which are denoted as Crack B. These are intended to initiate and propagate under the action of the stress component in y direction.

Fig. 11 shows the photos of blast-induced cracks formed in the three

Table 1
Attenuation index under different cavity volume conditions.

	0-L	V-L	2V-R	3V-R	4V-R
Attenuation index of the first strain peak/n_1	1.48	1.76	2.04	1.78	1.48
Attenuation index of the second strain peak/n_2	2.25	2.36	2.32	2.68	2.19

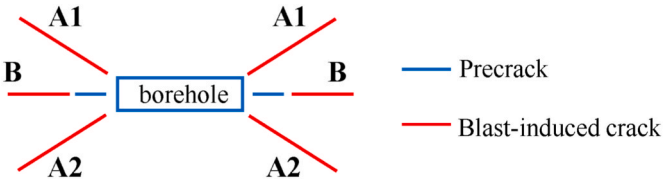

Fig. 10. Schematic diagram of the distribution of blast-induced cracks around borehole after blasting.

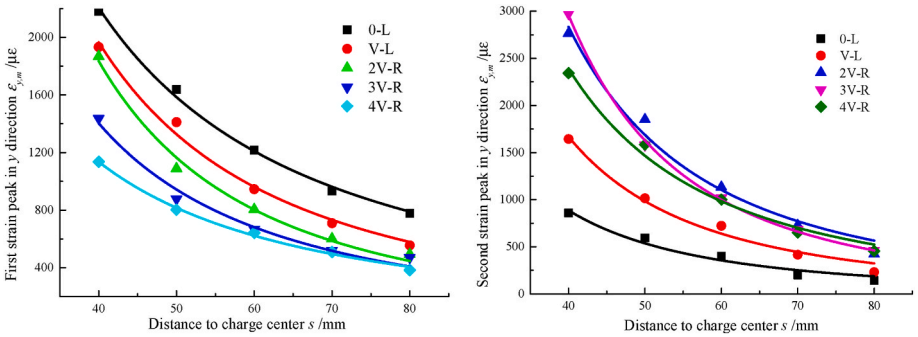

(a) First strain peak (b) Second strain peak

Fig. 9. Attenuation curve of strain peak with distance.

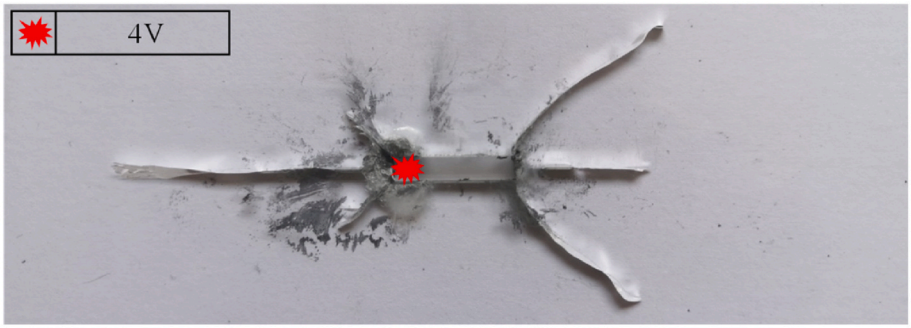

(a) Specimen T1

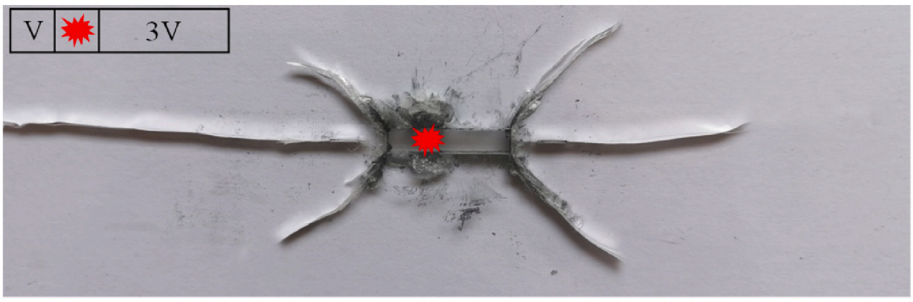

(b) Specimen T2

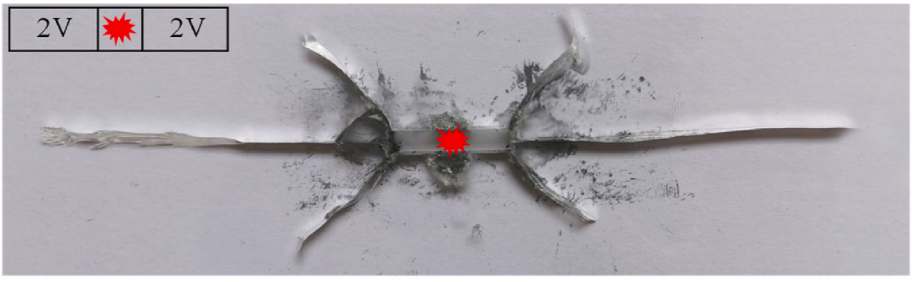

(c) Specimen T3

Fig. 11. Photos of blast-induced cracks in all the considered specimens after blasting.

Table 2
Length of blast-induced crack under different cavity volume conditions.

	0	V	2V	3V	4V
Length of A1/mm	10.1	19.4	20.2	24.7	31.8
Length of A2/mm	11.6	21.3	21.0	24.9	28.3
Average length of A1 and A2/mm	10.9	20.4	20.6	24.8	30.1
Length of B/mm	35.7	53.6	47.8	29.7	12.1

groups of specimens after blasting. It can be found that the charge position has a significant effect on the distribution of blast-induced cracks. Since the stress states of Crack A1 and Crack A2 under blasting are the same, the propagation paths and lengths of Crack A1 and Crack A2 are essentially the same. The statistics of blast-induced crack length under different cavity volume conditions are listed in Table 2, and from this, the changing curve of the length of blast-induced crack with cavity volume shown in Fig. 12 is drawn. The formation of Crack A1 and Crack A2 is mainly caused by the stress concentration effect. With the increase of cavity volume, the action effect of blasting stress wave is reduced, and the action time of blasting gas is prolonged. This prevents excessive fragmentation of the medium around borehole and provides longer-term

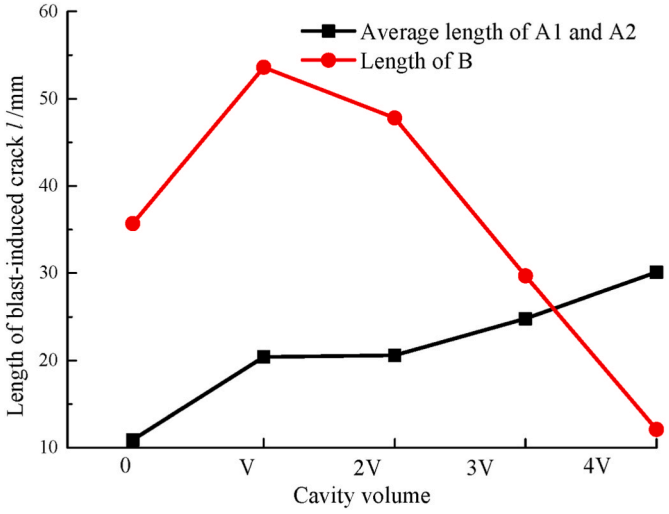

Fig. 12. Changing curve of length of blast-induced crack with cavity volume.

dynamic support for the propagation of Crack A1 and Crack A2. This causes the propagation lengths of Cracks A1 and Crack A2 to gradually increase. Crack B mainly propagates under the action of the stress component (tensile stress) in *y* direction. According to the previous analysis results, the stress component in *y* direction has two peaks, wherein the first peak is caused by the action of blasting stress wave, and the second peak is formed by the action of blasting gas. The first peak decreases rapidly with the increase of cavity volume, while the second peak increases first and then decreases with the increase of cavity volume. The second peak is strong and lasts for a long time, thus becoming the main driving force for the propagation of Crack B. This further establishes that the length of Crack B increases first and then decreases with the increase of cavity volume.

5. Conclusions

In the present study, a cavity charge structure is proposed, which helps in quantitatively distinguishing the effects of blast stress wave and blast gas over the time and space scales. The main conclusions are as follows:

The time and space action characteristics of blasting gas can be controlled by modifying the borehole charge structure and creating a cavity between the charge and the borehole wall. This enables obtaining the "double-peak" evolution law of blasting strain. The first peak is generated by the direct impact of the detonation wave on the borehole wall, and the second peak is generated by blasting gas impacting the borehole wall after diffusing in the cavity. The second peak follows the first peak after a delay, and the effects of blasting stress wave and blasting gas are distinguished over the time and space scales.

The relative position of the charge in borehole dictates the volume of the cavity on either side of the charge, which affects the evolution of blasting strain. With the increase of the cavity volume, the first peak value of the stress component in *y* direction gradually decreases, while the second peak value increases first and then declines. This characterizes various influence mechanisms of the cavity on blasting stress wave and blasting gas effect. Furthermore, the attenuation of the strain peak under the action of blasting gas is more rapid.

The relative position of the charge affects the propagation and distribution of blast-induced cracks as well. The pressure in the borehole progressively redistributes as the cavity volume rises, and the propagation length of crack caused by the stress concentration at the four corners of borehole gradually increases. The crack propagation on the left and right sides of borehole is dominated by the stress component in *y* direction. With increasing cavity volume, the propagation length initially increases and subsequently decreases. It can be seen that in the cavity charge structure, the space-time effect of blasting stress wave and blasting gas can be effectively utilized to achieve controllable rock fragmentation by altering the charge location and cavity volume. In engineering practice, air-spaced charges are generally used in open pit bench blasting. The research results will provide new ideas for the charge structure design in open pit bench blasting.

Compliance with ethics guidelines

Chenxi Ding, Renshu Yang, Cheng Chen, Xinguang Zhu, Chun Feng and Quanmin Xie declare that they have no conflict of interest or financial conflicts to disclose.

Declaration of competing interest

The authors declare that they have no known competing financial interests or personal relationships that could have appeared to influence the work reported in this paper.

Data availability

Data will be made available on request.

Acknowledgments

This research was supported by: (1) National Natural Science Foundation of China (52204085, 51934001); (2) Interdisciplinary Research Project for Young Teachers of USTB (Fundamental Research Funds for the Central Universities) (FRF-IDRY-21-006); (3) Fundamental Research Funds for the Central Universities (FRF-TP-20-044A1); (4) Foundation of Hubei Key Laboratory of Blasting Engineering (BL2021-05); (5) China Postdoctoral Science Foundation (2021M700386).

References

1 Torbica S, Lapcevic V. Rock breakage by explosives[J]. *Eur Int J Sci Technol*. 2014;3(2):96–104.
2 Langefors U, Kihlström B. *The Modern Technique of Rock blasting[M]*. New York: Wiley; 1963.
3 Fourney WL, Dick RD, Wang XJ, Wei Y. Fragmentation mechanism in crater blasting [J]. *Int J Rock Mech Min Sci*. 1993;30(4):413–429.
4 Kutter HK, Fairhurst C. On the fracture process in blasting[J]. *Int J Rock Mech Min Sci*. 1971;8:181–202.
5 Chu HB, Yang XL, Hou AJ, Yu YQ, Liang WM. A simulation-based experimental study on explosion stress wave propagation and attenuation in coal[J]. *Explos Shock Waves*. 2012;32(2):185–189 ([in Chinese]).
6 Zhang ZX. *Rock Fracture and Blasting: Theory and Applications[M]*. Oxford: Butterworth-Heinemann; 2016.
7 Zhang ZX, Chi LY, Qiao Y, Hou DF. Fracture initiation, gas ejection, and strain waves measured on specimen surfaces in model rock blasting[J]. *Rock Mech Rock Eng*. 2021;54:647–663.
8 Zhang ZX, Qiao Y, Chi LY, Hou DF. Experimental study of rock fragmentation under different stemming conditions in model blasting[J]. *Int J Rock Mech Min Sci*. 2021;143, 104797.
9 Ding CX, Yang RS, Feng C. Stress wave superposition effect and crack initiation mechanism between two adjacent boreholes[J]. *Int J Rock Mech Min Sci*. 2021;138, 104622.
10 Yang RS, Ding CX, Yang LY, Lei Z, Zheng CD. Study of decoupled charge blasting based on high-speed digital image correlation method[J]. *Tunn Undergr Space Technol*. 2019;83:51–59.
11 Cho SH, Kaneko K. Rock fragmentation control in blasting[J]. *Mater Trans*. 2004;45(5):1722–1730.
12 Yang XL, Wang MS. Mechanism of rock crack growth under detonation gas loading [J]. *Explos Shock Waves*. 2001;21(2):111–116 ([in Chinese]).
13 Banadaki MMD, Mohanty B. Numerical simulation of stress wave induced fractures in rock[J]. *Int J Impact Eng*. 2012;40(2):16–25.
14 Yang RS, Ding CX, Yang LY, Lei Z, Zhang ZR, Wang YB. Visualizing the blast-induced stress wave and blasting gas action effects using digital image correlation[J]. *Int J Rock Mech Min Sci*. 2018;112:47–54.
15 Ding CX, Yang RS, Lei Z, Chen C, Zheng CD. Experimental study on blasting energy distribution and utilization efficiency using water jet test[J]. *Energies*. 2020;13:5340.
16 Trivino LF, Mohanty B. Assessment of crack initiation and propagation in rock from explosion-induced stress waves and gas expansion by cross-hole seismometry and FEM-DEM method[J]. *Int J Rock Mech Min Sci*. 2015;77:287–299.
17 Ma GW, An XM. Numerical simulation of blasting-induced rock fractures[J]. *Int J Rock Mech Min Sci*. 2008;45:966–975.
18 Aliabadian Z, Sharafisafa M, Mortazavi A, Maarefvand P. Wave and fracture propagation in continuum and faulted rock masses: distinct element modeling[J]. *Arabian J Geosci*. 2014;7:5021–5035.
19 Yan CZ, Sun GH, Zheng H, Ge XR. Simulation of explosive gas-driven rock fracture by FEM/DEM[J]. *Rock Soil Mech*. 2015;36(8):2419–2425 ([in Chinese]).
20 Lin YS, Zhang BK, Jiang JB, Liu ZN, Ding YS. Mechanism and influencing factors on radial fractures' cracking and propagation under exploding gas[J]. *Petrol Drill Tech*. 2008;36(3):50–54 ([in Chinese]).
21 Yue ZW, Zhou J, Feng C, Wang X, Peng LZ, Cong JY. Coupling of material point and continuum discontinuum element methods for simulating blast-induced fractures in rock[J]. *Comput Geotch*. 2022;144, 104629.
22 Ding CX, Yang RS, Lei Z, Wang M, Zhao Y, Lin H. Fractal damage and crack propagation in decoupled charge blasting[J]. *Soil Dynam Earthq Eng*. 2021;141, 106503.
23 Yang RS, Ding CX, Yang LY, Lei Z, Zheng CD. Study of decoupled charge blasting based on high-speed digital image correlation method[J]. *Tunn Undergr Space Technol*. 2019;83:51–59.
24 Yu WL, Wang T, Gao YL. *Basics of Explosive Gas Dynamics[M]*. Beijing: Ordnance Industry Press; 2007.